

# Rapid Prototyping Materials Rheology

T. E. Karis, D. J. Dawson

IBM Research Division, Almaden Research Center, 650 Harry Road, San Jose, CA 95120

C. R. Davis

Johnson Filaments, 36 Industrial Avenue, Williston, VT 05495

R.-N. Kono, G. Kim, and M. S. Jhon

Department of Chemical Engineering, Carnegie Mellon University, 5000 Forbes Avenue, Pittsburgh, PA 15213

S. J. Kim

Samsung Advanced Institute of Technology, Suwon, Korea

---

A new technology for printing three-dimensional solid objects from computer-generated images is described. The technology is based on extrusion of a thermoplastic polymer melt as small fibers that bond to form the solid object. This technology is referred to as thermoplastic melt extrusion rapid prototyping (RP). Polymer materials for thermoplastic melt extrusion RP must have the ability to form the structural building blocks of the part. These building blocks are walls, shelves, and bridges. The flow and deformation (rheology) of the melt as it is extruded through the circular die and adheres to the layers already in place govern the process. At this exploratory stage of development, there is no model to specify the extrusion conditions and materials properties relationship to RP performance. Ten marginally acceptable RP materials were identified through extensive RP testing. This study presents the preliminary rheological and thermal analytical characterization of these materials. Characterization of the melt properties is fundamental to the development of a constitutive equation for modeling and to an understanding of the process. The most promising RP materials were found to be crystallizing polymers. Isothermal rheometry and calorimetry measurements were performed to study the crystallization kinetics. Solidification due to crystallization during extrusion is expected to play a key role in RP materials performance.

Journal of Imaging Science and Technology 40: 147 – 154 (1996)

---

## Introduction

Rapid prototyping (RP) is an emerging technology that promises the ability to print computer data files as three-dimensional physical objects. There are numerous approaches to rapid prototyping. Several rapid prototyping devices are commercially available. For example, cross sections of an object can be printed on two-dimensional media. The object is then built by assembling successive cross sections. RP can be performed by stereolithographic means in which a laser scans a photosensitive polymer resin, which crosslinks to form a solid object. This study

considers a new RP technique in which a thermoplastic polymer is extruded from the melt to form the solid object.<sup>1,2</sup> The thermoplastic melt extrusion RP technique offers the advantages of safety through the use of nontoxic polymers, increased processing speeds, improved resolution of the object, and lower cost.

In thermoplastic melt extrusion RP, the polymer melt is stored in a heated reservoir. Fibers are extruded from a circular die that is typically several hundred micrometers in diameter. The die assembly and/or the sample stage translates in three dimensions as the fibers are extruded. The fibers adhere to one another as they cool and solidify. The structural building blocks in thermoplastic melt extrusion RP are *walls*, *shelves*, and *bridges*. Walls are made when the fibers are extruded on top of one another. Shelves are made by extruding fibers alongside one another. Bridges are made by extruding fibers across the free space between two walls. The ability of a material to make the structural building blocks, as well as to fulfill the requirements of the finished part, requires specific material properties in both the melt and solid state. The melt temperature must also be low enough to minimize burn hazards and odor. The melt viscosity must be adequate for flow from the reservoir into the extrusion nozzle under moderate pressure. The melt must thicken as it is extruded from the die to maintain the shape of the fiber. The fibers should remain tacky long enough to bond with the adjacent fibers. The completed part must be sufficiently stiff to allow handling and assembly with other parts in a large model. It cannot be so brittle that it is easily broken if dropped. The melting point of the thermoplastic must be high enough to avoid softening by normal exposure to sunlight.

There are challenges to be overcome before thermoplastic extrusion RP is a viable tool. Appropriate polymers, composites, and/or blends that satisfy the requirements must be custom made or selected from a large number of available materials. The extrusion setup conditions must be determined for each material. A large number of tests is required for each new material to identify the optimum setup conditions of melt temperature, barrel temperature profile, nozzle diameter, flow rate, etc. RP performance must be evaluated for each set of conditions by making test parts. The ability of a material and setup to make the functional building blocks is observed. The walls must be

---

Original manuscript received April 2, 1995. Revised January 4, 1996.

©1996, IS&T—The Society of Imaging Science and Technology

free of curl so that they remain straight upon cooling. The shelves must remain horizontal without drooping. The bridges must extend across free space without slumping or sagging. In the absence of a model for determining the relationship between performance, melt properties, and setup conditions, a large number of tests are required. Each new material candidate must be evaluated for its performance over the whole range of setup conditions to determine an operating “window.”

Prior to this study, a large number of RP material candidates were evaluated. Materials from which parts could be made were identified. None of the materials satisfied all of the performance requirements. Further progress in the area of thermoplastic extrusion RP technology relies on the development of a general design model. A numerical simulation model is desirable to assist in determining the optimum combination of setup conditions and material properties. Commercial software is available for modeling conventional extrusion processes. A new model and simulation code are required specifically for the extrusion RP process, taking into account the fiber deformation and adhesion downstream from the nozzle while the material cools to room temperature. Polymer flow and solidification modeling require a constitutive equation that describes the properties of the materials being extruded. Melt rheology and thermal analysis of the RP materials are needed to develop the appropriate constitutive equation for modeling.

The objective of this study is to characterize the melt rheology and thermal analysis of the RP materials and to identify the material properties that must be incorporated into a constitutive equation. Thermal analysis is employed to determine the glass transition, melting, and crystallization temperatures. Melt rheology is used to characterize the flow properties during cooling from the melt. During the course of this study, we found that some of the most promising RP material candidates crystallized during cooling. Consequently, additional rheological and thermal analytical tests were used to study the crystallization kinetics. Correlation between the material properties and RP performance is the subject of another study.

## Experimental

**Materials and Apparatus.** The materials studied were commercially available polyamides, polyesters, and hot melt

adhesives. Table I lists the samples and their transition temperatures. Measurement of these transition temperatures is described below. Most of the rheological measurements were done using a stress rheometer [Carrimed (now TA Instruments) Model CSL500] with a high-temperature oven. The fixture was a 2 cm diameter, 1° angle cone with a 28  $\mu\text{m}$  gap. The isothermal rheological measurements were performed with a mechanical spectrometer (Rheometrics, Model RMS 705) with a melt oven. The fixture was a pair of 2.5 cm diameter parallel plates with a 1 mm gap. Thermal analysis was performed by a differential scanning calorimeter (DSC) (DuPont, Model 2100).

**Procedure.** In the temperature sweep test, the material was heated above its melting temperature,  $T_m$ , for 3 min. The material was cooled at an average rate of 20°C/min in 5°C increments while measuring  $G'$  and  $G''$  (storage and loss modulus) at each temperature. The oscillation frequency,  $\omega$ , was 1 rad/s and the strain amplitude,  $\gamma$ , was 1%. The temperature was decreased until the material became too stiff for measurable angular displacement.  $G'$  and  $G''$  increased sharply at some point as the temperature was being lowered. The temperature at which the modulus reached  $10^7$  dyne/cm<sup>2</sup> is referred to as the *solidification temperature* of the material,  $T_s$  in Table I.

In the strain amplitude sweep test, the material was heated above  $T_m$  and cooled to 20°C above  $T_s$ .  $G'$  and  $G''$  were measured at  $\omega = 1$  rad/s as  $\gamma$  was increased from 1 to 15%. This test was repeated after heating the material above  $T_m$  and cooling to 10°C above  $T_s$ . Dependence of  $G'$  and  $G''$  on  $\gamma$  signals the presence of nonlinear viscoelastic effects. In the absence of crystallinity, the materials were linearly viscoelastic up to more than 10% strain.

In the oscillation frequency sweep test, the material was heated above  $T_m$  and cooled to 20°C above  $T_s$ . The moduli  $G'$  and  $G''$  were measured over a range of  $\omega$  from 251 to 0.251 rad/s. The material was heated above  $T_m$ , cooled to 10°C above  $T_s$ , and  $G'$  and  $G''$  were measured over the same range of  $\omega$ . The oscillation frequency sweep test was intended to provide data for the master curve of the oscillation frequency dependence of  $G'$  and  $G''$ . The master curve is used to calculate the relaxation time spectrum of thermoplastic polymer melts. For glass-forming polymers such as polystyrene, a log–log plot of the melt moduli at different temperatures can be superimposed by shifting along the frequency axis

**TABLE I. RP Samples Tested and their Solidification Temperatures  $T_s$  from Rheometry and Melting Temperatures  $T_m^i$  ( $i=1,2,3$ ) from Differential Scanning Calorimetry**

Material	Chemical type	Transition temperatures (°C)			
		$T_s$	$T_m^1$	$T_m^2$	$T_m^3$
6G	Copolyester	40	135		
2247	Nylon copolymer	50			
114T	Terpolymer of Nylon 6, Nylon 6/6, and Nylon 12	50	40*	90*	115*
80-20	Ethylene vinyl acetate; FORAL blend	65	65	95	
1330	Polyamide	80	130		
3759	Polyamide	90		90–140	
ABS	Acrylonitrile-butadiene-styrene	120			
5039	Polyamide	125	130		
Polyacetal	Polyoxymethylene copolymer	155	165		
NYL11	Nylon 11	170	190		

\*RP extruded sample

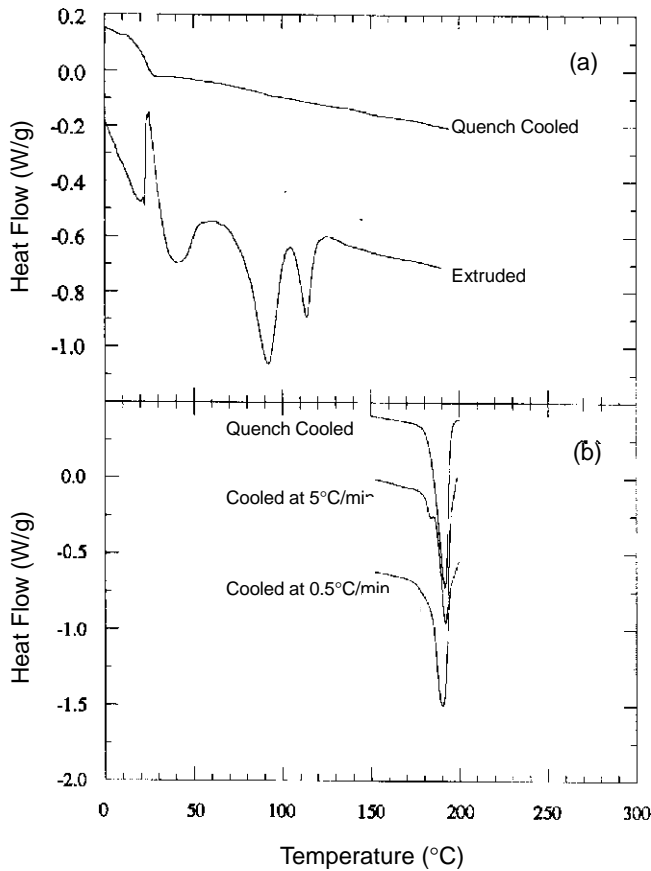


**Figure 1.** Heat flow as a function of temperature in the DSC measurement: (a) 114T and (b) NYL11. Heating rate 10°C/min.

until the curves at each temperature overlap one another. The plot of shifted data is referred to as the *master curve*. Frequency-temperature superposition was not possible for most of the RP materials because of crystallization.

Creep and recovery tests were done on each material under the same temperature conditions as the frequency sweep tests. In the creep and recovery test, the creep compliance  $J(t)$  (strain/stress) is measured while a constant stress is applied (creep) and after the stress is removed (recovery). Constant stress was applied for 60 s to measure the creep. The recovery was measured for 30 s after removal of the stress. The linear slope of the steady-state compliance plotted as a function of time is inversely proportional to the low shear rate melt viscosity. The recovery is a measure of the elastic energy storage in the melt.

In the shear stress sweep test, the shear stress was increased to its maximum value in 60 s and decreased to zero in 60 sec as in a thixotropic loop measurement. The material was heated above  $T_m$ , cooled to 20°C above  $T_s$ , and the shear rate was measured as a function of the shear stress. This test was repeated after heating the material above  $T_m$  and cooling to 10°C above  $T_s$ . The shear stress sweep test measures the viscosity dependence on shear rate. For most of the materials, this test could not be completed as a result of solidification due to crystallization. The shear stress sweep test provided no additional information on the melt properties, and the results are not shown.

In the isothermal rheometry test, the storage modulus was measured as a function of time at constant temperature to study the crystallization kinetics. The material was heated above  $T_m$ , rapidly cooled, and held at one temperature to observe the growth of crystallinity. Small-amplitude oscillatory shear at 1 rad/s and 1% strain amplitude

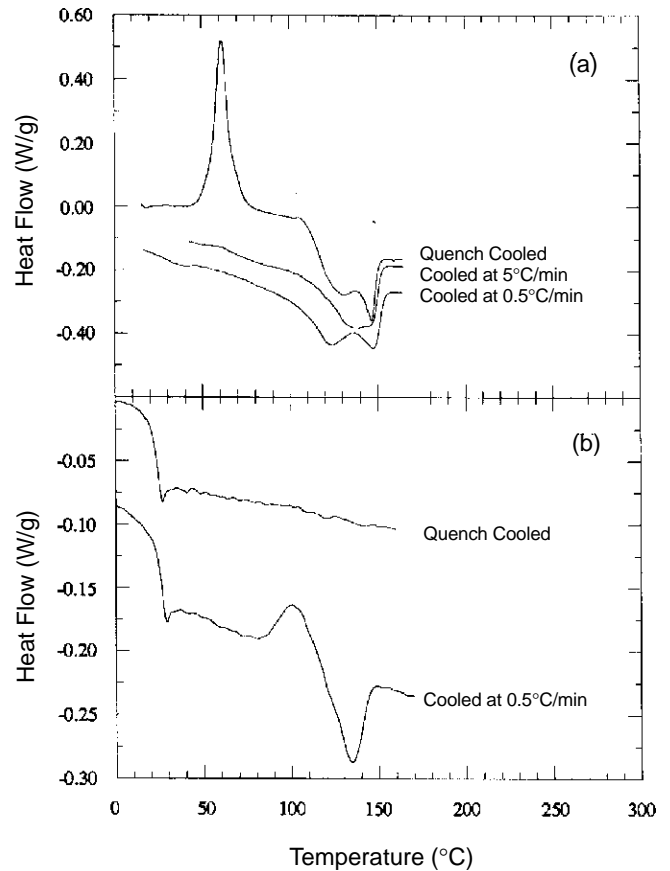


**Figure 2.** Heat flow as a function of temperature in the DSC measurement: (a) 5039 and (b) 6G. Heating rate 10°C/min.

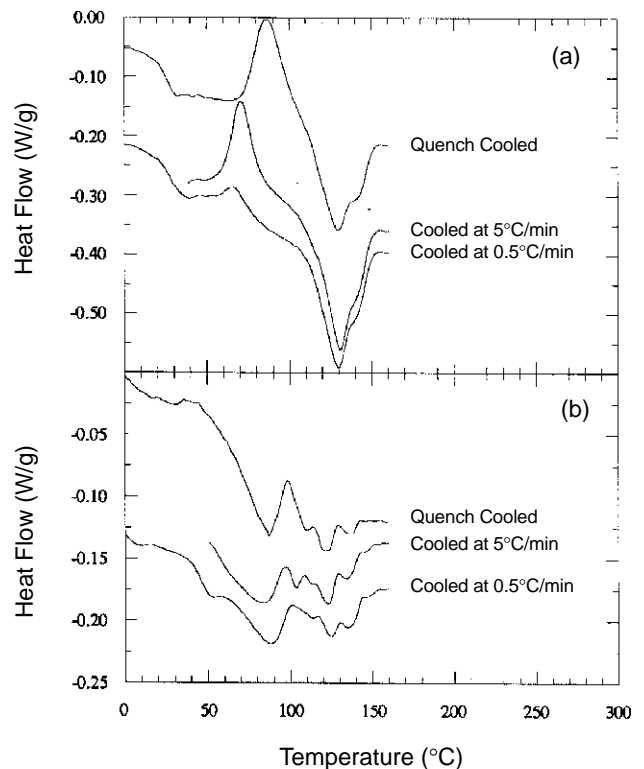


**Figure 3.** Heat flow as a function of temperature in the DSC measurement: (a) 1330 and (b) 3759. Heating rate 10°C/min.

was applied while the storage modulus was periodically measured as the sample crystallized. This procedure was repeated at several temperatures. The results were used to determine the crystallization curves. Application of a preshear at a shear rate of 0.1 or 1.0 s<sup>-1</sup> for 60 s at the isothermal temperature used to observe crystallization had no effect on the crystallization kinetics.

Thermal analysis using DSC was performed to study the crystallization kinetics. Nonisothermal DSC measurements were used to characterize the melting properties and crystallization. The procedure is as follows: (1) heat from room temperature to 200°C at 10°C/min, (2) quench cool on a liquid nitrogen cooled metal plate, (3) heat at 10°C/min, (4) cool at 5°C/min, (5) heat at 10°C/min, (6) cool at 0.5°C/min, and (7) heat at 10°C/min. The heat flow was recorded during each heating at 10°C/min to study the heat flow due to the glass transition and crystal growth and melting. The melting temperatures  $T_m$  from DSC are listed in Table I. Typical nonisothermal DSC results are shown in Figs. 1 through 3.

Isothermal DSC was used to measure crystallization in the melt by recording the heat flow as a function of time at a number of fixed temperatures in the vicinity of  $T_s$ . The heat of crystallization gave rise to a clearly observable exotherm for a number of the RP materials. An example of isothermal DSC is shown in Fig. 4.

## Results and Discussion

**Melt Rheology.** Typical temperature sweep rheological data are shown in Fig. 5. The 114T in Fig. 5(a) has a lower  $T_s$  than the NYL11 in Fig. 5(b). One cannot tell whether the material was glass forming or crystallizing from these curves alone without the use of complementary DSC measurements. The nature of the transition in the moduli with decreasing temperature approaching  $T_s$  is identified as being either smooth or sharp in Table II. As a glass-forming polymer melt approaches its glass transition temperature

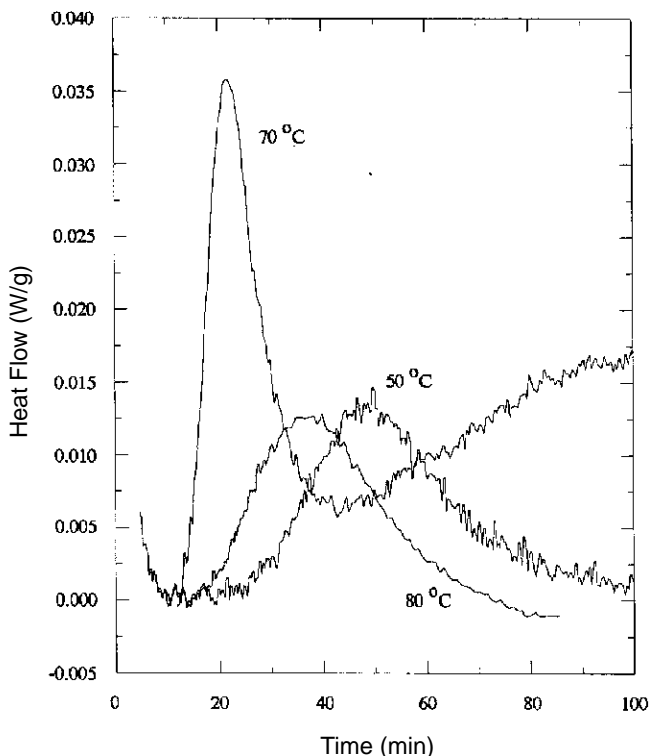


**Figure 4.** Heat flow as a function of time in the isothermal DSC measurement for quench-cooled 114T.

from a higher temperature, the moduli increase smoothly according to an exponential function of temperature such as that described by the Vogel–Tammann–Fulcher or Williams–Landell–Ferry equations.<sup>3</sup> This type of relation was found in a number of the materials. In contrast, some of the materials exhibited a sharp transition in the moduli with decreasing temperature. This sharp transition is typically observed when a melt crystallizes.

Oscillation frequency sweep data were obtained by heating above  $T_m$  followed by rapid cooling and measurement at two different temperatures 10 and 20°C above  $T_s$ . The results of the frequency sweep tests at temperatures in the neighborhood of  $T_s$  were complicated by the occurrence of crystallization in the melt, so that the master curves could not be made. Typical results from these tests are shown on log-log plots of  $G'$  versus  $G''$  in Fig. 6. For a linearly viscoelastic liquid,  $G'$  plotted as a function of  $G''$  on log-log coordinates should lie on a smooth curve with a slope of 2 at low  $G'$ . Data taken at different temperatures should overlap one another on this curve. Deviation from this ideal behavior by the RP materials, as illustrated in Fig. 6, could be due to structural changes in the materials during the test (e.g., crystallization). The relationship between  $G'$  and  $G''$  is discussed by Han and Jhon,<sup>4</sup> and the relationship between  $G'$ ,  $G''$ , and contact adhesion is discussed by Chang.<sup>5</sup>

Typical creep and recovery test results are shown in Fig. 7. Points to the left of the dashed line were measured during the application of stress, and points to the right were measured after the stress was removed. For some of the samples, the creep could not be measured because the

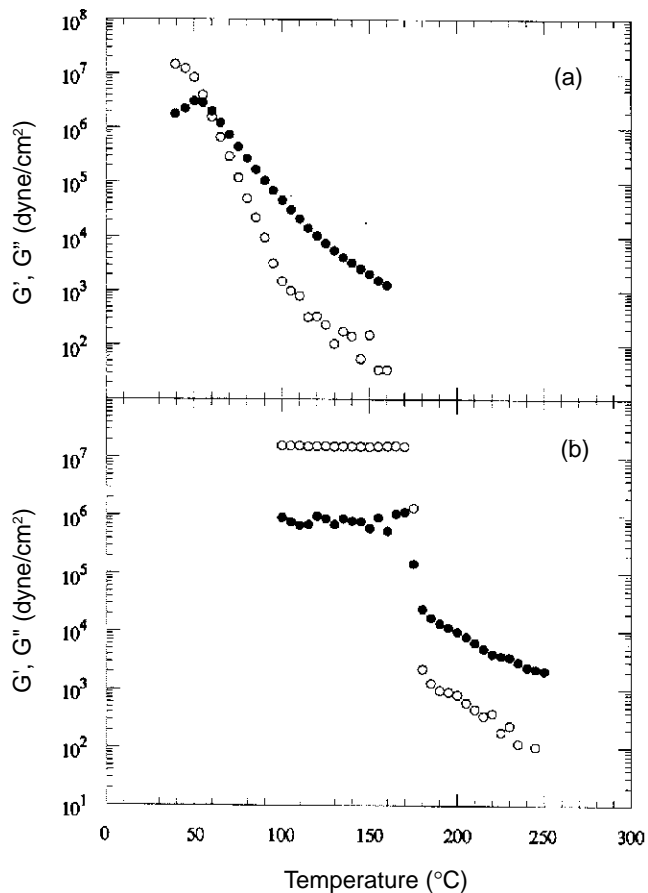


**Figure 5.** The storage modulus  $G'$  (O) and the loss modulus  $G''$  (•) as a function of temperature in the temperature sweep measurement: (a) 114T and (b) NYL11.

**Table II. Viscoelastic Properties of the RP Materials\***

Material	150°C						
	$G' \times 10^{-2}$ (dyne/cm <sup>2</sup> )	$G'' \times 10^{-2}$ (dyne/cm <sup>2</sup> )	tan $\delta$	$\eta_0 \times 10^{-2}$ (poise)	$J_e^0 \times 10^5$ (cm <sup>2</sup> /dyne)	$\tau_c$ (s) (sec)	Solidification transition
6G	4	10	25	10	40	0.4	Smooth
2247	1	80	80	80	0.16	0.01	Smooth
114T	0.7	20	29	20	1.8	0.04	Smooth
80-20	1	1	1	1	1000	1	Smooth
1330	60	700	12	700	0.12	0.8	Smooth
3759	0	5	25	5	8	0.04	Sharp
ABS	2	4000	0.4	4000	0.63	2.5	Smooth
5039	10000	20	20	20	2.5	0.05	Sharp
200°C							
Polyacetal	40	600	15	600	0.11	0.07	Sharp
NYL11	9	100	11	100	0.9	0.09	Sharp

\*Oscillation Frequency  $\omega = 1$  rad/s

sample crystallized and became solid during the test. These tests were intended to measure the elastic recovery in the melt. Significant elastic recovery was observed only with the 80–20, 3759, and ABS materials.

Well above  $T_m$ , most of the materials behaved as viscous liquids ( $G'' \gg G'$ ). Two exceptions were the 80–20 and ABS. The loss tangent, defined as  $\tan \delta = G''/G'$ , is

listed in Table II. The viscoelastic properties of zero shear viscosity  $\eta_0$ , steady-state recoverable compliance  $J_e^0$ , and characteristic time  $\tau_c$  were estimated, using

$$G'(\omega) = \omega^2 \eta_0^2 J_e^0, \quad G''(\omega) = \omega \eta_0, \quad \text{and} \quad \tau_c = \eta_0 J_e^0. \quad (1)$$

The viscoelastic properties calculated from  $G'$  and  $G''$  and Eq. 1 are also listed in Table II.

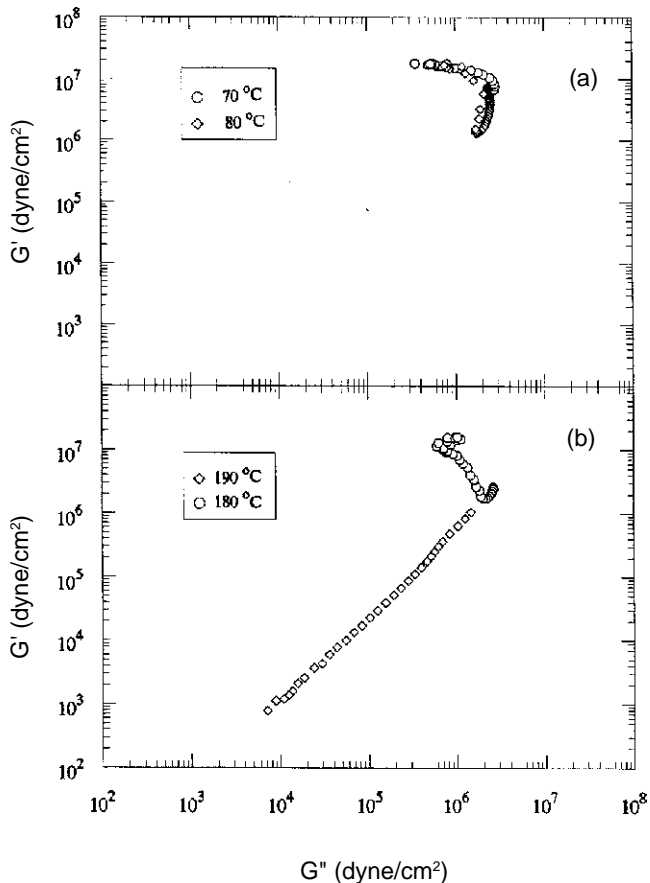


**Figure 6.** The storage modulus  $G'$  as a function of the loss modulus  $G''$  in the frequency sweep measurement: (a) 114T and (b) NYL11.

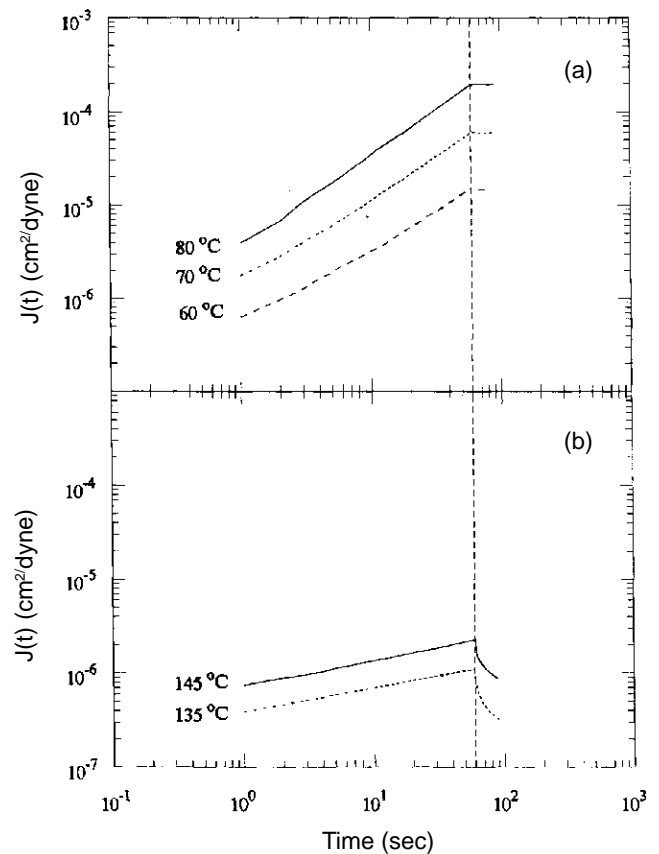


**Figure 7.** The creep compliance as a function of time during stress application (to the left of the dashed line) and recovery after stress removal (to the right of the dashed line): (a) 114T and (b) ABS.

**Thermal Analysis.** Crystallization, which has such a dramatic effect on the rheological properties, was studied by observing the DSC heating curves. The materials were melted and cooled at three different rates, followed by heating to observe any glass transition, crystallization exotherm, and melting endotherm. Most of the RP materials examined had a tendency to form a glass when quench cooled and to crystallize when slowly cooled or during heating. Crystallization during cooling shows up as a melting endotherm during subsequent heating at 10°C/min. Crystallization during cooling was studied by cooling at different cooling rates and observation of the heating curve.

The DSC heat flow is illustrated in Figs. 1 through 3. The DSC heat flow curves for the two materials that had the best (114T) and the worst (NYL11) performance are shown in Fig. 1. The heat flow for the quench-cooled 114T while heating at 10°C/min is the upper trace in Fig. 1(a). The glass transition shows up near 25°C, and there are no transitions with increasing temperature. The lower curve in Fig. 1(a) is the heat flow for 114T that was subject to RP extrusion. In this case, no glass transition was observed. Several crystallization exotherms and melting endotherms occurred. The glass transition was replaced by a sharp growth exotherm near 25°C. The remaining structure in the heat flow curve for the RP-extruded 114T exhibits crystal growth exotherms near 55 and 105°C, and crystal melting endotherms near 40, 90, and 115°C. The heat flow for the extruded 114T was significantly different from that of the quench-cooled material. These differences may be due to one or more of the following: a slower cooling rate during extrusion, shear-induced crystallization during extrusion, or surface nucleation on carbon

black pigment particles in the extruded material. The presence of the multiple crystallization growth exotherms indicates several forms of crystal structure, each with its own nucleation and growth rate.

The remaining materials were preconditioned and tested, following the steps given in the experimental procedure. The DSC heat flow for the NYL11 is shown in Fig. 1(b). Even quench-cooled NYL11 had only a single melting endotherm, indicating complete crystallization during quench cooling.

The DSC heat flow for the 5039 is shown in Fig. 2(a), and that for the 6G is shown in Fig. 2(b). The 5039 quench-cooled without significant crystallization, because the crystal growth took place during heating, as indicated by the sharp growth exotherm near 60°C. Complete crystallization occurred in the 5039 during cooling at the slower rates, as shown by the absence of the growth exotherm during heating and about the same enthalpy of crystal melting near 130°C as in the quench-cooled sample. The 6G of Fig. 2(b) quench-cooled to form a glass, and the quench-cooled sample did not crystallize during heating. The sample cooled at 0.5°C/min, shown in the lower trace in Fig. 2(b), formed a glass but also exhibited crystal growth and melting upon heating. This may be due to the formation of nuclei during cooling at the slower rate.

The DSC heat flow for the 1330 is shown in Fig. 3(a), and that of the 3759 is shown in Fig. 3(b). The 1330 quench cooled to form a glass and crystallized near 85°C upon heating. Increased crystallization took place during cooling at the slower rates, as shown by the reduction in the area of the growth exotherm with decreasing cooling rate.

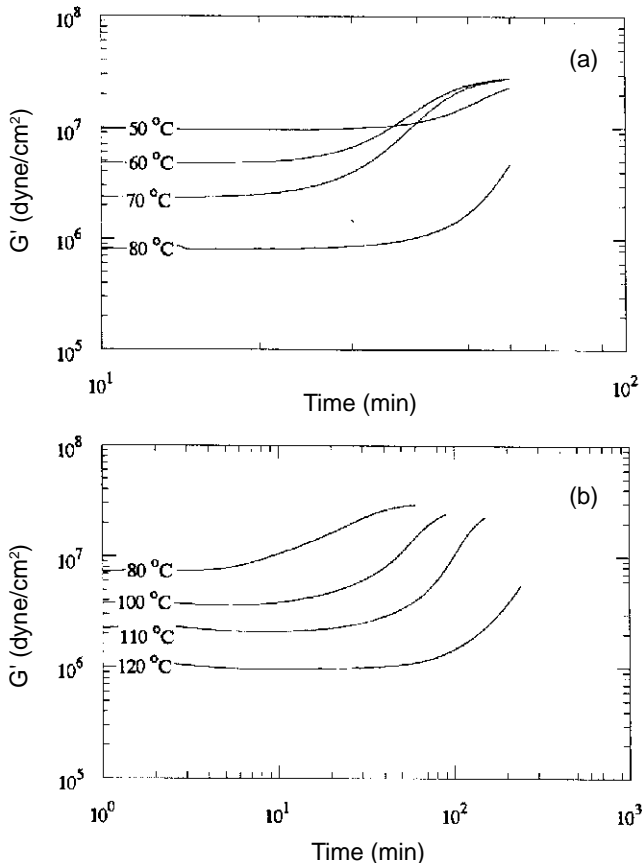


**Figure 8.** The storage modulus  $G'$  as a function of time in the isothermal rheometry measurement: (a) 114T and (b) 1330.

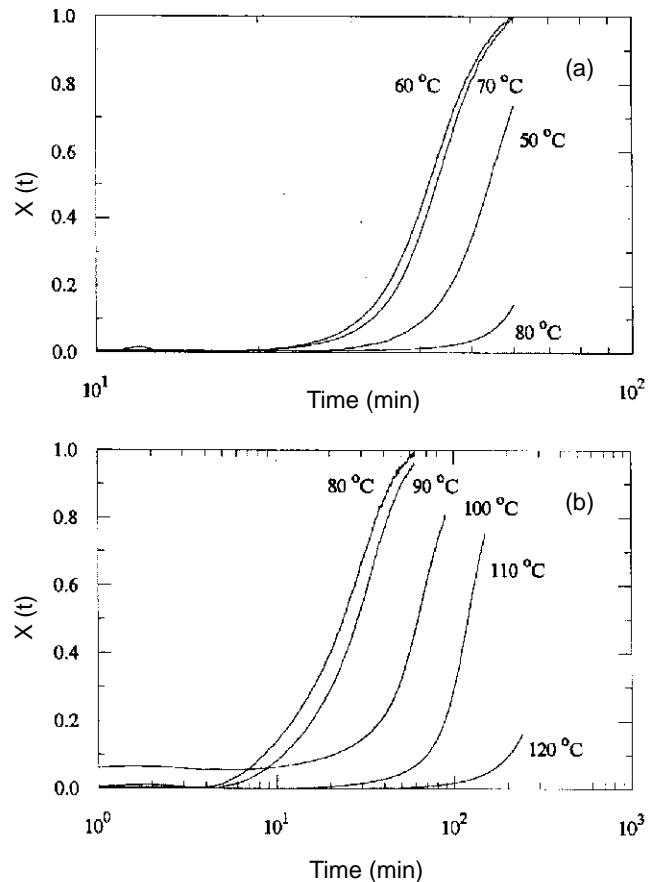


**Figure 9.** Relative volume fraction crystallinity as a function of time at isothermal temperatures calculated from the isothermal rheometry data in Fig. 8, using Eq. 3: (a) 114T and (b) 1330.

The 3759 of Fig. 3(b) showed a similar tendency to crystallize during cooling at the slower rates. There appears to be more than one form of crystals present in the 3759, indicated by the complicated structure of the heat flow between 90 and 140°C.

The melting temperatures  $T_m$ , or temperature ranges, from the DSC heating curves for the RP materials are listed in Table I along with the rheologically determined solidification temperatures  $T_s$ . In all cases  $T_s \leq T_m$ , which is consistent with undercooling of the crystallizing component, leading to the onset of crystal growth and solidification during cooling.

**Crystallization Kinetics.** To characterize the tendency of the melt to crystallize during cooling, the time-temperature transformation (TTT) curves of the materials were indirectly measured, using isothermal rheometry and calorimetry. TTT curves are used to present the degree of crystallinity in the materials subjected to a known thermal history. The TTT curve is plotted with coordinates of temperature on the vertical axis and time on the horizontal axis. The curve is selected to follow a given volume fraction of crystallinity, or an isocrystallinity line. Each point on the isocrystallinity line is obtained by suddenly cooling the sample from the melt and holding it at a temperature where crystals will grow at a finite rate. The degree of crystallinity is recorded as a function of time until the fraction of crystals reaches the value for which the isocrystallinity line is being plotted, e.g., 10%.

The isothermal crystallization data are described by the Avrami equation:

$$X(t) = 1 - \exp(-kt^n). \quad (2)$$

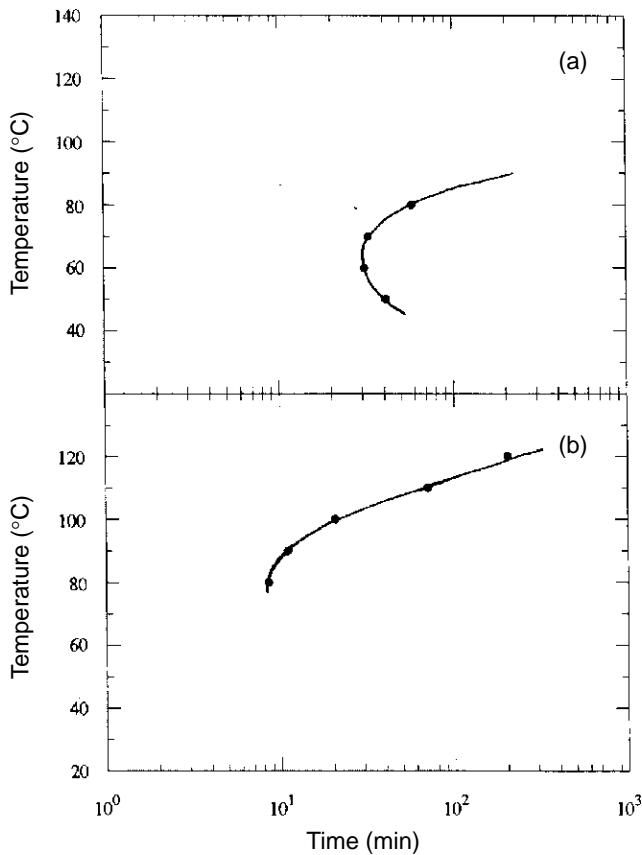


**Figure 10.** The TTT diagram calculated from the isothermal rheometry data. The time is that needed for the relative crystallinity to reach 10%: (a) 114T and (b) 1330. The lines show the general curve shape expected for crystallization from an undercooled melt.

The Avrami equation relates the volume fraction of crystals,  $X(t)$ , to time  $t$ . In Eq. 2,  $k$  is the crystallization rate constant<sup>6,7</sup> and is a function of temperature;  $n$  is the Avrami index, which is related to the crystal growth mechanism; and  $X(t)$  can be measured by x-ray diffraction. In the following analysis of the isothermal rheometry and calorimetry data to estimate  $X(t)$ , the methods used to interpret the data provide only the volume fraction of crystals relative to the amount of crystallization that takes place in the sample rather than the absolute volume fraction of crystals in the material.

The growth of crystallinity in the melt was studied by measuring  $G'$  as a function of time over a temperature range in which there is a finite crystallization rate. Figure 8 illustrates the evolution of  $G'$  after rapidly cooling from above  $T_m$  and holding at a constant temperature above  $T_s$ . The examples given are for the 114T [Fig. 8(a)], and the 1330 [Fig. 8(b)]. The value of  $X(t)$  is calculated from the storage modulus,  $G'(t)$ , by

$$X(t) = \frac{G'(t) - G'(0)}{G'(\infty) - G'(0)}, \quad (3)$$

where  $G'(0)$  and  $G'(\infty)$  are the initial and the asymptotic values of the storage modulus, respectively. The variation of  $X(t)$  with time is shown in Fig. 9. The time when  $X(t) = 0.1$  at each temperature was used to generate the TTT diagram. Figure 10 shows the TTT diagrams for 114T

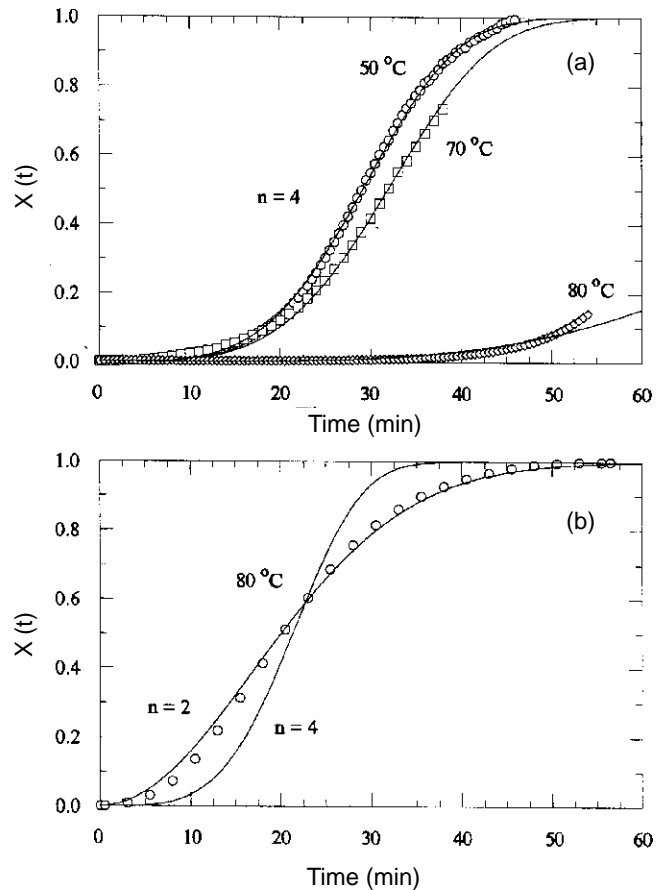


**Figure 11.** Relative volume fraction crystallinity as a function of time for 114T calculated from (a) isothermal rheometry data and (b) isothermal DSC data. The solid lines show the regression fit to the Avrami equation, Eq. 2, with the indicated values of  $n$ .

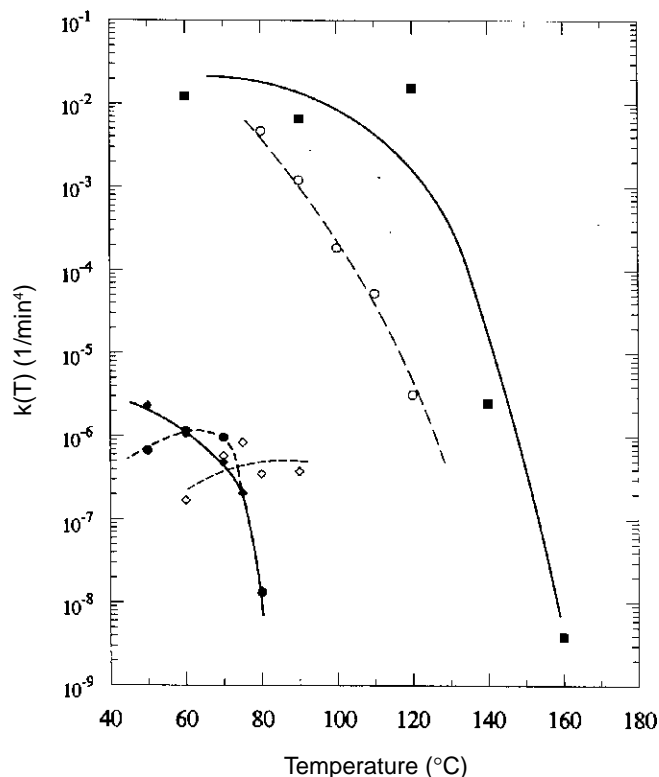


**Figure 12.** Crystallization rate constant from the isothermal rheometry data: ● 114T, ○ 1330, ◇ 6G, ◆ 2247, and ■ 5039.

[Fig. 10(a)], and 1330, [Fig. 10(b)]. The values of  $n$  and  $k$  were calculated from the  $X(t)$  by a least squares fit to Eq. 2. An example of the curve fit to  $X(t)$  measured by isothermal rheometry is shown in Fig. 11(a) for the 114T. Here the data were shifted along the time axis by  $t_0$  to make  $X(0) = 0$ . For some of the curve fits, the values of  $n$  were fixed to integer values of 2, 3, or 4. The example of the curve fit shown in Fig. 11(a) was calculated with  $n = 4$ . The best fit of Eq. 2 to the isothermal rheometry crystallization data was obtained with  $n = 4$  at all temperatures ( $n = 4$  implies a three-dimensional growth mechanism). The crystallization rate constant  $k$  calculated from the isothermal rheometry data with  $n = 4$  is plotted as a function of temperature in Fig. 12 for the RP materials that exhibited measurable crystallization.

The relative crystallinity can also be calculated from the heat flow during crystallization, measured by isothermal DSC. Figure 4 shows the heat flow for the 114T at three different temperatures. Here the relative crystallinity was determined from the exothermic peaks using the following relation:<sup>8</sup>

$$X(t) = \frac{\int_0^t \text{Heat Flow}(t) dt}{\int_{-\infty}^{\infty} \text{Heat Flow}(t) dt} \quad (4)$$

Baseline drift was subtracted when performing the integration. The  $X(t)$ -versus-time data curves for 114T at 80°C are shown in Fig. 11(b). The  $X(t)$  calculated from the isothermal DSC data could not be fit with  $n = 4$ . The best fit was obtained with  $n = 2$ , as shown in Fig. 11(b) ( $n = 2$  is consistent with one-dimensional growth, and is in agreement with the literature values<sup>9</sup> for similar materials).

The crystallization of the 114T at 80°C took place much more rapidly during the isothermal DSC measurement [Fig. 11(b)] than it did during the isothermal rheometry measurement [Fig. 11(a)]. The  $n$  from rheometry was 4 and the  $n$  from calorimetry was 2. The differences between the calorimetry and rheometry, are as follows: The sample surface area-to-volume ratio is higher in the DSC than in the rheometer, and the sample is quiescent in the DSC, whereas it is being sheared in the rheometer. Crystallization rates in sheared melts have previously been reported as being greater than those in quiescent melts.<sup>10,11</sup> Further tests should investigate the shear effects on crystallization<sup>12</sup> during RP extrusion. The crystallization kinetics should be incorporated in modeling the RP extrusion process, using a coupled flow and heat transfer model.

## Summary and Conclusions

The requirements of materials for an RP process using thermoplastic fiber extrusion were described. A large number of materials were evaluated prior to this study. Some of the materials could be used to make parts but they still lacked adequate performance. A numerical model for the materials and process setup conditions for extrusion is needed. The melt properties of the most promising candidate materials were characterized to determine the most important properties to incorporate into a constitutive equation for modeling. The most significant observation was the tendency of the RP materials to crystallize from the melt. Whereas the constitutive equation should treat the cooling melt as a viscoelastic liquid undergoing a transition to a viscoelastic solid, it must also take into account the time and temperature history dependence of the fluid properties resulting from crystallization.

A qualitative description of the materials response determining RP performance may be given as follows. The polymer starts out as a melt in the reservoir. The melt flows into the extrusion die, which may be held below the melt temperature. Cooling begins in the die, with the development of a radial temperature gradient. The center of the fiber remains at a higher temperature than the surface. Crystallization begins to occur at a rate that depends on radial position in the fiber, die temperature profile, and extrusion velocity. The fiber stiffness at the exit of the die is determined by the distribution of crystallinity and proximity to the glass transition temperature. The ability of the fiber to bridge and shelve without slumping is determined by the fiber stiffness, which may be enhanced by a higher degree of crystallinity in the core of the fiber. The presence of curl during wall formation is expected to depend on the relaxation of frozen-in stress on cooling during flow through the die and volume change during cooling through the glass transition temperature. ▲

**Acknowledgment.** We are grateful for the support and encouragement of J. Batchelder throughout this study. The thermal analysis was done under the thoughtful guidance of R. Siemens.

## References

1. S. S. Crump, Modeling apparatus for three-dimensional objects, US Patent 5,340,433, Aug. 1994.
2. J. S. Batchelder, H. W. Curtis, D. S. Goodman, F. Gracer, R. R. Johnson, G. M. Koppelman, and J. D. Mackay, Model generation system having closed-loop extrusion nozzle positioning, US. Patent 5,303,141, Apr. 1994.
3. J. D. Ferry, *Viscoelastic Properties of Polymers*, 3rd ed., Wiley, New York, 1980.
4. C. D. Han and M. S. Jhon, Correlations of the first normal stress difference with the shear stress and the storage modulus for homopolymers, *J. Appl. Polymer Sci.*, **32**: 3809 (1986).
5. E. P. Chang, Viscoelastic windows of pressure-sensitive adhesives, *J. Adhesion*, **34**: 189 (1991).

6. R. M. Patel, and J. E. Spruiell, Crystallization kinetics during polymer processing—Analysis of available approaches for process modeling, *Polymer Eng. and Sci.* **31** (10): 730 (1991).
7. D. R. Uhlmann and N. J. Kreidl, *Glass: Science and Technology*, Academic Press, London, 1983, pp. 1–47.
8. C. Bas, P. Battesti, and N. D. Alberola, Crystallization and melting behaviors of poly(aryletheretherketone) (PEEK) on origin of double melting peaks, *J. Appl. Polymer Sci.*, **53**: 1745 (1994).
9. T. Limtasiri, S. J. Grossman, and J. C. Huang, Kinetic studies of the crystallization of Nylon-6 block copolymers, *Polymer Eng. and Sci.* **29** (8): 493 (1989).
10. C.-M. Hsiung, M. Cakmak, and J. L. White, Crystallization phenomena in injection molding of polyetheretherketone, and its influence on mechanical properties, *Polymer Eng. and Sci.* **30** (16): 967 (1990).
11. J. E. Spruiell and J. L. White, Structure development during polymer processing: Study of the melt spinning of polyethylene and polypropylene fibers, *Polymer Eng. and Sci.*, **15** (9): 660 (1975).
12. G. S. Y. Yeh and K. Z. Hong, Strain-induced crystallization, part III: Theory, *Polymer Eng. and Sci.* **19** (6): 395 (1979).